A kinetic Monte Carlo study of vacancy diffusion in non-dilute Ni-Re alloys

Goswami, Kamal Nayan; Mottura, Alessandro

DOI:
10.1016/j.msea.2018.11.064

Document Version
Peer reviewed version

Citation for published version (Harvard):
Goswami, KN & Mottura, A 2018, 'A kinetic Monte Carlo study of vacancy diffusion in non-dilute Ni-Re alloys', *Materials Science and Engineering A*. https://doi.org/10.1016/j.msea.2018.11.064

A kinetic Monte Carlo study of vacancy diffusion in non-dilute Ni-Re alloys

Kamal Nayan Goswami[a], Alessandro Mottura[a,*]

[a]*School of Metallurgy and Materials, The University of Birmingham, Edgbaston, Birmingham B15 2TT, United Kingdom*

Abstract

The beneficial effect of Re on the creep strengthening properties in single crystal Ni-based superalloys is well known, albeit understanding the underlying mechanism is still an ongoing area of investigation. The microstructure in these alloys comprises of cuboids of the hard precipitate phase embedded in a softer matrix phase. At high temperatures, the glide of creep dislocations is restricted to the matrix only, and dislocation climb is required to get around a precipitate. Vacancy diffusion is an essential component of dislocation climb and elements like Re which are slow-diffusing in Ni are expected to affect this phenomenon. In the present work, we aim to study this by calculating the effect of Re composition on the rate of vacancy diffusion in Ni using kinetic Monte Carlo simulations. First principles electronic structure calculations based on density functional theory have been used to calculate the thermodynamic and kinetic parameters in both dilute as well as non-dilute alloys. Results suggest appreciable modification of the vacancy diffusion coefficients, indicating that the beneficial role of Re in Ni-based superalloys can be largely explained by its effect on vacancy diffusion.

Keywords: Ni-based superalloys, Re-effect, vacancy diffusion, kinetic Monte Carlo simulations

1. Introduction

Ni-based superalloys represent a class of materials designed to withstand extreme conditions [1]. Their excellent performance under high temperature creep conditions, amongst others, make them suitable for applications such as in turbine blades in gas turbine engines used for jet propulsion in civil and military aircrafts. From thermodynamic considerations, high engine efficiencies are achieved at high operating temperatures and over the past few decades, the improvements in superalloy technology have raised the temperature capability of the gas turbine engines beyond 1273 K [1]. This has mostly been achieved by altering the chemical composition of these superalloys considerably. The addition of Re, a rare and expensive metal, in particular was seen to have a strong creep strengthening effect. But even as the improvement in strength is clearly seen, an understanding of the fundamental mechanism leading to the observed strengthening is still lacking [2]. High temperature creep is dependent on the rate of vacancy diffusion and an accepted argument within the superalloys community is that slow diffusing atoms, like Re, slow down the vacancy

*Corresponding author
Email address: a.mottura@bham.ac.uk (Alessandro Mottura)

diffusion, leading to the lowering of creep deformation rate [2, 3]. Other important elements like Ta, W and Mo are also potent strengtheners, albeit to a lesser degree.

Single crystal Ni-based superalloys, simply put are γ-γ' alloys where γ phase is the random substitutional solid solution of Ni and γ' phase is the Ni_3Al based ordered phase with a $L1_2$ structure [1]. The γ phase forms a continuous matrix in which cuboidal precipitates of γ' phase are embedded in a coherent manner with its <001> crystallographic direction aligned to the <001> crystallographic direction of the γ phase. Re, the subject of the current study, strongly partitions to the γ phase and has a dramatic effect on improving the creep lives of superalloys [4]. Across a wide range of temperature and stress combinations in the tertiary creep regime, the deformation in Ni-based superalloys is restricted to the thin γ channels [1]. The gliding dislocations do not penetrate the γ' precipitates and hence they have to climb around them at the γ/γ' interfaces for deformation to continue. Depending on the microstructure and the loading direction, the dislocations have to either climb up or down. The upward dislocation climb is associated with the absorption of vacancies, while the downward dislocation climb is associated with the emission of vacancies [5]. This creates a simultaneous flux of vacancies from the emitting dislocation cores to absorbing dislocation cores. Slow diffusing solutes such as Re partitions to the γ phase where it could act as strong hindrances to the diffusion of vacancies.

Constitutive creep models commonly show that the minimum creep strain rate, $\dot{\epsilon}$ is proportional to an effective diffusion factor D_{eff}, which is thought to be strongly influenced by chemistry such as the presence of slow-diffusing atoms [5, 6].

$$\dot{\epsilon} \propto D_{\text{eff}} \tag{1}$$

However, there is no unique formulation for calculating D_{eff} [7–10]. Our hypothesis is that the vacancy diffusion coefficient D_{v} is proportional to the effective diffusion coefficient D_{eff} and hence is an equivalent measure of D_{eff}. This is because the diffusion of vacancies in the γ matrix in one direction means the simultaneous diffusion of atoms (predominantly Ni) in the reverse direction. However, it must be kept in mind that vacancies have to diffuse for much longer distances through the lattice compared to the individual atoms and hence D_{eff} and D_{v} would differ by orders of magnitude. Nevertheless, the relative effect of the alloy composition on D_{v} should be the same as D_{eff}.

Our previous work [11] was based on the use of an analytical model for vacancy diffusion developed by Manning [12] and indicated that small additions of slow-diffusing atoms in a Ni lattice do not reduce the diffusion rate of vacancies substantially. However, Manning's model is based on a number of simplifying assumptions which undermine the validity of the results. On the other hand, Schuwalow et al [13] have calculated the vacancy diffusion coefficients for solutes in Ni using a combination of first principles calculations and kinetic Monte Carlo simulations. They concluded that within the dilute limits, interactions between the vacancies and solute atoms were too weak to have a net effect at the relevant temperatures. But they also suggested that consideration of solute-solute interactions were necessary to account for the local fluctuations in solute concentration, especially given the partitioning behaviour of solutes within

the γ-γ' structure. The present work thus aims at investigating the effect of Re additions in the non-dilute range on the vacancy diffusion in Ni using kinetic Monte Carlo simulations in an attempt to explain the observed Re-effect as well as to generate meaningful diffusion data for future alloy design programmes.

2. Methodology

2.1. Kinetic Monte Carlo simulations

Analytical methods for the rigorous calculation of diffusion coefficients in non-dilute alloys cannot be formulated given the complexity of the problem, however some approximate models do exist in the literature [14–17]. This problem is solved using the kinetic Monte Carlo (kMC) methods which simulate the dynamical evolution of a system over time at a particular temperature [18]. The trajectories of the atoms and vacancy as a result of individual diffusive jumps are tracked throughout the simulation. The rate constant associated with an individual diffusive jump is defined within the transition state theory as [19]

$$\Gamma_i = \nu_i^* \exp\left\{-\frac{\Delta E_{\mathrm{m},i}}{k_\mathrm{B} T}\right\} \tag{2}$$

where ν_i^* is the effective frequency associated with the vibration of the atom i in the direction of the vacancy [19] , $\Delta E_{\mathrm{m},i}$ is the migration energy or the activation energy barrier given by the difference between the energy at the saddle point (activated state) and the starting point of the transition, k_B is the Boltzmann constant and T is the absolute temperature. In kMC simulations, only the diffusive exchange between an atom and a vacancy are treated while the atomic vibrations about their equilibrium positions are suitably averaged [20, 21]. The algorithm for a kMC simulation to calculate the diffusion coefficients is described elsewhere [22]. At the end of the desired number of diffusive jumps, for a kMC simulation cell containing a single vacancy, the vacancy diffusion coefficient D_v is calculated using

$$D_\mathrm{v} = \frac{1}{6}\frac{\partial}{\partial t}\left\langle R_\mathrm{v}^2(t)\right\rangle \tag{3}$$

and the solute diffusion coefficient D_i using

$$D_i = \frac{x_\mathrm{v}}{x_\mathrm{v}^{sim}} \times \frac{1}{6N}\frac{\partial}{\partial t}\sum_{i=1}^{N}\left\langle\left[R_i^2(t)\right]\right\rangle \tag{4}$$

where $\left\langle R^2(t)\right\rangle$ is the squared displacement of the vacancy (or solute atoms) from the initial state, N is the number of i atoms, t is the time elapsed, x_v is the actual vacancy concentration [11] at temperature = T , while x_v^{sim} is the vacancy concentration used in the kMC simulation. $R^2(t)$ is calculated as

$$R^2(t) = |x(t) - x(0)|^2 + |y(t) - y(0)|^2 + |z(t) - z(0)|^2 \tag{5}$$

where the values on the right represent the coordinates of the vacancy(or solute atoms) at time = t and time = 0.

The kMC simulation should be run for a sufficiently large number of steps such that the D values converge. To obtain better statistics, the kMC trajectory is divided over a number of segments and D calculated from the time-weighted averages of the diffusion coefficients calculated from the various segments [13, 23]. In the case where an

atom or a vacancy does not perform a true 'random walk', its jump is said to be correlated and its correlation factor f is given as [24],

$$f = \frac{2}{n}\frac{\left\langle R^2(t)\right\rangle}{a^2} \tag{6}$$

where a is the Ni lattice parameter and n is the number of jumps.

For the case of dilute alloys, only a few activation energy barriers are needed to describe the system. However in the case of non-dilute alloys, atoms can be arranged in a number of configurations. This means a number of activation energy barriers corresponding to these atomic configurations need to be calculated, which is difficult. This problem is made simpler by using the cluster expansion method.

2.2. Cluster Expansion

The cluster expansion can be seen as a generalised Ising Model [25] . The lattice of a binary alloy such as Ni-Re can be represented using occupation variables (σ_i) [26–28]. For example, in the present work a value of +1 represents a Ni atom, while -1 represents a Re atom. The vector of the occupation variables $\vec{\sigma}$ would then uniquely describe the configuration of the system. The energy of the alloy E for a configuration $\vec{\sigma}$ can be expanded using polynomials ϕ_α of σ_i

$$E(\vec{\sigma}) = V_0 + \sum_\alpha V_\alpha \phi_\alpha(\vec{\sigma}) \tag{7}$$

where ϕ_α is simply the product of occupation variables belonging to a particular cluster of sites α, *i.e.* $\phi_\alpha = \prod_{i\in\alpha}\sigma_i$. These clusters could be point clusters, pairs, triplets, quadruplets... etc. The expansion of this equation to an infinite number of clusters theoretically should describe the energy exactly. However, the expansion is usually truncated up to a few clusters which can describe the energy to a reasonable precision. V_α are the effective cluster interaction (ECI) coefficients and are calculated by fitting energy calculated from first principles for a number of configurations [29]. Thus, from a relatively small first principles dataset, the energy for any given configuration can be cluster expanded using this technique.

Vacancies can be treated as a perturbation to the binary cluster expansion[30] since their concentration in an alloy is small even at high temperatures. An effective vacancy formation energy (EVFE) for a vacancy at site i is defined as [30],

$$\Delta E_i^{\text{eff}} = E_i^{\text{v}}(\vec{\sigma}) - \frac{1}{2}\left[E_i^{\text{Ni}}(\vec{\sigma}) + E_i^{\text{Re}}(\vec{\sigma})\right] \tag{8}$$

This EVFE can be parametrised using a local cluster expansion using coefficients which only depend on the local Ni-Re configuration. $E_i^{\text{v}}(\vec{\sigma})$ is the desired energy of the alloy with a vacancy and is obtained by rearranging the Equation 8. $E_i^{\text{Ni}}(\vec{\sigma})$ and $E_i^{\text{Re}}(\vec{\sigma})$ are the energies when the vacancy is replaced by a Ni atom or a Re atom, and these can be calculated from the usual binary cluster expansion.

The activation energy barriers were also cluster expanded locally using a formalism similar to EVFE. The activation energy barriers not only depend on the surrounding configuration, but also on the direction of the jump. Hence to get around this, kinetically resolved activation (KRA) barriers were defined as [31],

$$\Delta E_{\mathrm{KRA}} = E_s - \frac{1}{2}\left(E_i + E_f\right) \tag{9}$$

where E_s is the energy of the activated state (saddle point), while E_i and E_f are the energy of the initial state and the final state (2 end points) of the jump . ΔE_{KRA} is thus independent of the direction of the jump, and can be cluster expanded locally. Once the KRAs and the energies of the end states are available, the activation energy barriers ΔE_m can be calculated as,

$$\Delta E_m = E_s - E_i = \Delta E_{KRA} + \frac{1}{2}\left(E_f - E_i\right) \tag{10}$$

Thus the cluster expanded energy of the binary alloy, the EVFE and the KRAs together would describe the Ni-Re system completely. These numbers are then fed into the kMC simulation to calculate the diffusion coefficients in the non-dilute regime.

2.3. Computational details

All input data were calculated from first principles, using DFT [32, 33] as implemented in the Vienna *Ab initio* simulation package (VASP) 5.3.2 [34]. The projector augmented wave (PAW) method [35, 36] was used to describe the electron-ion interactions, and the generalized gradient approximation (GGA) parameterised by Perdew, Burke and Ernzerhof [37] was used as E_{XC}. All calculations were performed on 108-atom supercells and were spin-polarized. The electronic self-consistent loops were stopped when the total energy converged to within 10^{-6} eV and ionic positions were relaxed until all forces fell below 10^{-2} eV/Å. The conjugate-gradient algorithm was used to relax the atoms in to their instantaneous ground states. A Methfessel-Paxton smearing width [38] of 0.1 eV was used. Calculations were run using an energy cutoff of 400 eV and $5 \times 5 \times 5$ k-point mesh following the Monkhorst-Pack scheme [39].

The migration barriers were calculated using the 'climbing image' nudged elastic band (CI-NEB) method [40, 41] using a single image. For these calculations, a spring constant value of 5 eV/Å^2 was used and only the internal degrees of freedom of the supercells were relaxed. The supercell size was fixed to the calculated lattice parameter value for pure Ni, a of 3.52 Å. The total energies change only by about ± 0.03 eV when the supercell volume and shape relaxations were taken into account. For all other calculations, besides the internal degrees of freedom of the supercells, the volume and the shape of the supercells were relaxed as well. The effective frequencies were calculated within the harmonic approximation as supported by VASP and have been presented in our previous work [11]. The cluster expansion was performed using the CASM code (Cluster-Assisted Statistical Mechanics) developed by the Van der Ven Research Group at the University of Michigan [27, 28].

3. Results and Discussion

3.1. Effective cluster interaction coefficients

A primitive *fcc* cell with configurational degree of freedom was given as the input to generate Ni-Re configurations in the entire binary composition space for maximum 10 atom supercells. 87 *fcc* supercells with a total of 2146 symmetrically distinct configurations were generated. Among these 2146 configurations, all possible configurations for supercells containing up to 4 atoms were selected while for bigger supercells, the configurations with Re concentration $\leq$ 20 at.% were selected. This was done to bias the cluster expansion to predict energies more accurately in the Ni-rich region. Thus, a total of 144 configurations were selected and their first principles energy was calculated. The cell volume, shape and all the internal degrees of freedom were relaxed. A $37 \times 37 \times 37$ k-point mesh was used for the primitive *fcc* cell. This has the same k-spacing in the reciprocal lattice [42] as a $5 \times 5 \times 5$ k-point mesh for a 108 atom *fcc* supercell which has been used for CI-NEB calculations in this work. To maintain the same k-spacing, the k-mesh was automatically adjusted for the different configurations depending on their lattice vectors. The formation energy per atom E_{form} of these 144 configurations were calculated according to the equation,

$$E_{\text{form}} = \frac{E_{\text{Ni}_x\text{Re}_y} - xE_{\text{Ni}} - yE_{\text{Re}}}{(x+y)} \tag{11}$$

where $E_{\text{Ni}_x\text{Re}_y}$ is the energy of the configuration Ni_xRe_y, x and y being the number of Ni and Re atoms respectively. E_{Ni} and E_{Re} are the energy of pure Ni and pure Re (calculated from first principles) used as reference states (see Table 2). Since all the configurations used in the present work were *fcc*, the energy for *fcc* Re was used as the reference. It must be noted that pure Re exhibits an *hcp* structure, however, in the Ni-rich regions, Re is expected to be present in an *fcc* solution of Ni. Amongst all the 144 configurations considered, the stoichiometric compound Ni_4Re at 20 at.% Re with a $D1_a$ structure was the lowest energy configuration with a formation energy of -0.073 eV. This was similar to the results of Maisel et al [43] and Levy et al [44] who calculated a formation energy of -0.058 eV and -0.064 eV respectively for Ni_4Re from their first principles calculations.

101 of these configurations were used to fit the ECIs for the cluster expansion. Configurations with a formation energy greater than 0.03 eV were discarded as their formation is less likely energetically. Also, configurations towards the Ni-rich side were preferred. Specifically, the configurations with a Re concentration greater than 33 at.% were discarded. This was partly because the concentration of Re in the γ phase even in the third generation of Ni-based superalloys never goes beyond 10 at.% [45]. It is unlikely that even the local composition in the γ phase due to statistical fluctuations would go beyond 33 at.%.

Clusters of maximum 3 atoms within a sphere radius of 6 Å were considered in the fitting of the effective cluster interaction coefficients. This meant a total of 27 possible clusters (1 empty cluster (V_0), 1 point cluster (V_α), 5 pair clusters (V_β) and 20 triplet clusters (V_γ)) were available for fitting the ECIs to the formation energy of the 101 configurations in the dataset. The fitting was done using the ecifit code incorporated within CASM. The ecifit code is a least squares fitting script combined with an implementation of a genetic algorithm [46] for determining the optimal

Table 1: The calculated effective cluster interaction coefficients (ECIs)

Clusters		ECIs (meV)	multiplicity	ECIs/multiplicity (meV)
empty (V_0)		-59.56	1	-59.56
point (V_α)		286.88	1	286.88
pairs(V_β)	1	-359.12	6	-59.85
	2	-0.97	3	-0.32
	3	-92.89	12	-7.74
	4	13.12	6	2.19
	5	-33.98	12	-2.83
triplets(V_γ)	6	91.40	8	11.42
	7	89.35	12	7.45
	8	-22.59	8	-2.82
	9	77.83	6	12.97
	10	128.56	48	2.68
	11	-54.52	12	-4.54
	12	-11.07	48	-0.23
	13	-31.09	24	-1.29

set of clusters to include. Sufficient accuracy was obtained when using a total of 15 clusters. The root mean square error between first-principles energies and cluster expanded energies for all 101 structures used in the fit was 5.7 meV per atom. This is a good fit considering the fact that an rms error value of 5.6 meV per atom was obtained by Van der Ven et al [30] using their ECIs calculated for Al-Li alloys.

Table 1 shows the fitted ECIs for Ni-Re. Five pair clusters (V_β) include the 1^{st} five nearest neighbour pairs. Eight triplet clusters (V_γ) have also been included. These pair and triplet clusters have been numbered 1 to 13 and Figure 1 represents these clusters. The empty cluster (V_0) is just a constant term used in the fitting while the point cluster (V_α) is the single atom cluster. Table 1 also shows the multiplicity of these clusters. For example, the pair cluster number 1 has a multiplicity of 6, meaning there are 6 symmetrically equivalent clusters in different orientations. This

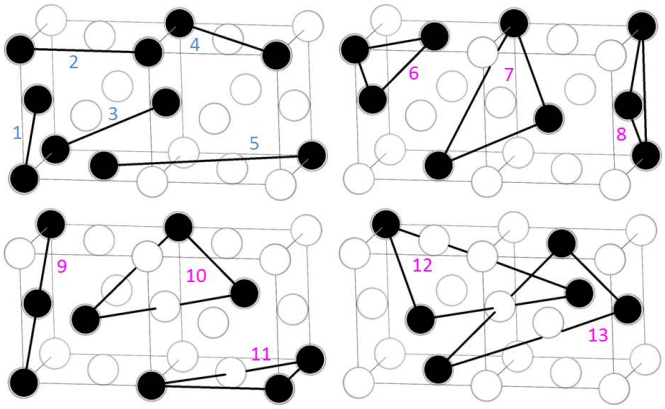

Figure 1: The pair clusters numbered 1 to 5 and triplet clusters numbered 6 to 13 used in the ECI fitting

Table 2: The first principles energy and energy predicted from cluster expansion of Ni-Re by the CASM code for pure Ni and pure Re

Reference state	FP energy (eV)	CE predicted energy (eV)
Ni	-5.48	-5.45
Re (*fcc*)	-12.34	-13.43

is expected as an atom in an *fcc* lattice is paired to twelve 1^{st} nearest neighbours, and each of these pairs is shared by 2 atoms. Hence, the multiplicity is 6. The ECIs/multiplicity have also been calculated as this is more suitable in our kinetic Monte Carlo code to model the energy of the Ni-Re alloys. As described earlier, an occupation variable (σ_i) value of +1 represents a Ni atom, while -1 represents a Re atom. It must be noted that the CASM code cluster expands the formation energy and not the total configurational energy. One can calculate the formation energy first from the obtained ECIs, and then the configurational energy can be deduced by rearranging the Equation (11).

Table 2 presents a comparison of the first principles energy and the energy predicted from cluster expansion using the above ECIs for pure Ni and pure Re (*fcc*). One can see that the match is very good for Ni, while there is a deviation of about 1 eV in the case of Re. This can be explained as only Ni-rich configurations were used to fit the ECIs. Nevertheless, we expect accurate prediction of the configurational energies in the composition range of interest (< 10 at. % Re). It must be clarified that the first principles energies for pure Ni and Re have been used to calculate the formation energies in Equation (11).

3.2. Effective vacancy formation energy

A local cluster expansion of the EVFE was done around one vacancy. Unlike the binary cluster expansion, where supercells of maximum 10 atoms were used, here first principles energy calculations were run on 3×3×3 supercells to avoid the vacancy-vacancy interaction across the periodic images. 26 different configurations were used and three calculations were performed on each of them, one with a vacancy at a lattice site ($E_i^v(\vec{\sigma})$) and two others with a Ni ($E_i^{Ni}(\vec{\sigma})$) and a Re ($E_i^{Re}(\vec{\sigma})$) atom each replacing that site. Thus 78 different calculations were performed in total. Configurations with upto 36 Re atoms (33 at.%) were considered in the calculations. For some of the non-dilute compositions considered, the ionic relaxation was terminated when the forces fell below 0.02 eV/Å. Also, a 4×4×4 k-mesh was used for these calculations.

The selection of clusters and the fitting of the corresponding ECIs for binary cluster expansion of the configurational energy in Ni-Re was performed using a genetic algorithm as incorporated in the CASM code. However, the option of local cluster expansion for the prediction of EVFE was not available with CASM. Hence, in this case, clusters were adopted from the work of Van der Ven et al [30]. Four point clusters (numbered 1 to 4) up to the 4^{th} nearest neighbour distance, and the 1^{st} nearest neighbour pair (numbered 5) and triplet clusters (numbered 6) around a vacancy were considered. LECIs corresponding to these clusters were fit using multiple regression and the results are tabulated in Table 3. It must be noted that the treatment of the cluster expansion is slightly different here, and instead of considering the occupation variables for all the atoms around a vacancy, the EVFE was fit to the number of

Table 3: The calculated local effective cluster expansion coefficients (LECIs)

Cluster No.	LECIs (meV)
1	57.14
2	-8.23
3	54.88
4	8.06
5	-54.13
6	131.21

Re atoms, Re pairs and Re triplets around a vacancy. The constant term was set as 10.2413 eV, which was the EVFE in pure Ni.

3.3. Kinetically resolved activation energy barriers

The kinetically resolved activation barriers were calculated for a number of vacancy pathways with different atomic environments. On top of the barriers considered for the dilute alloys of Ni-Re [13], other barriers based on the fourteen-frequency model [15] were considered. The barriers were calculated using the climbing image nudged elastic band method for the forward and the reverse jumps and the KRA was deduced from the two.

From definition, KRAs are independent of the direction of the jumping atom and they represent the saddle point energy normalised to the arithmetic mean of the energies of the two end points. Thus the occupation variables defined for the local cluster expansion for KRAs should be centred about the saddle point, in contrast to the local cluster expansion of EVFE, where the occupation variables were defined in relation to their distance from the vacancy. However, the saddle point does not overlap on a lattice site and lies approximately halfway between the jumping atom and the vacancy. Thus, the set of lattice positions at a certain distance from the jumping atom, and the set of lattice positions at the same distance from the vacancy are considered equivalent and are clubbed together. For example, the lattice positions which are 1^{st} nearest neighbours to either the jumping atom or the vacancy are considered equivalent.

For simplification, the kinetic effective cluster interaction coefficients (KECIs) in the present work were fit to the number of Re atoms around a saddle point instead of considering the occupation variables of all the atoms. It was assumed that the presence of Re atoms in the combined 1^{st} nearest neighbour shell of the jumping atom and the vacancy affect the barriers, while those beyond have no role to play. Four different point clusters were included in the present case. For a Ni atom performing a jump, the KRA was given by,

$$\Delta E^{\mathrm{Ni}}_{\mathrm{KRA}} = 1.08 + 0.108 \times N^{1,1}_{\mathrm{Re}} - 0.080 \times N^{1,2}_{\mathrm{Re}} - 0.004 \times N^{1,3}_{\mathrm{Re}} + 0.022 \times N^{1,4}_{\mathrm{Re}} \tag{12}$$

To explain this, Figure 2 should be referred which shows an *fcc* {111} plane with an atom (black) about to perform an exchange with a vacancy. There are a combined total of 18 atoms which are 1^{st} nearest neighbours to either the atom or the vacancy. $N^{1,1}_{\mathrm{Re}}$ represents the number of Re atoms which are 1^{st} nearest neighbours to both the jumping

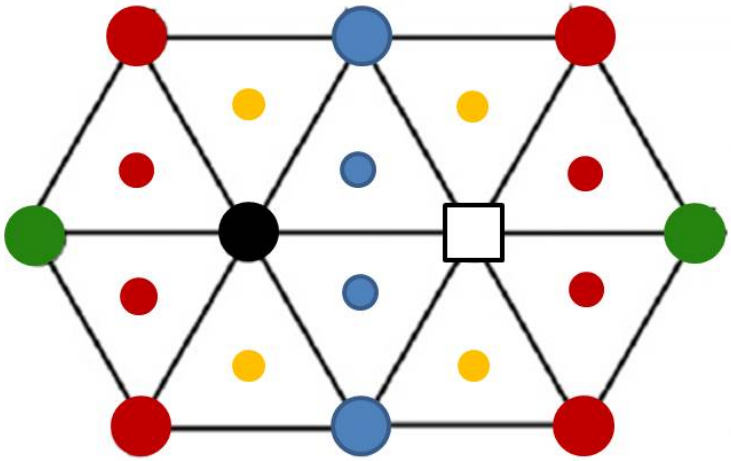

Figure 2: The *fcc* {111} plane showing an atom in black next to a vacancy surrounded by other atoms in the 1^{st} nearest neighbour shell. The colour of these atoms represent their relationship to the black atom and the vacancy. Atoms out of the plane have been shown smaller in size.

atom or the vacancy (blue positions), $N_{\mathrm{Re}}^{1,2}$ represents the number of Re atoms which are 2^{nd} nearest neighbours to either the jumping atom or the vacancy (yellow positions), $N_{\mathrm{Re}}^{1,3}$ represents the number of Re atoms which are 3^{rd} nearest neighbours to either the jumping atom or the vacancy (red positions) and $N_{\mathrm{Re}}^{1,4}$ represents the number of Re atoms which are 4^{th} nearest neighbours to either the jumping atom or the vacancy (green positions). Thus depending on which of these categories the Re atoms in the 1^{st} nearest neighbour shell belong to, we describe our KRA. If there are no Re atoms surrounding the jumping Ni atom, the KRA value is 1.08 eV from Equation 12, which is also the expected energy barrier in pure Ni.

For a Re atom performing a jump, the KRA was given by,

$$\Delta E_{\mathrm{KRA}}^{\mathrm{Re}} = 1.505 + 0.099 \times N_{\mathrm{Re}}^{1,1} + 0.007 \times N_{\mathrm{Re}}^{1,2} + 0.007 \times N_{\mathrm{Re}}^{1,3} + 0.007 \times N_{\mathrm{Re}}^{1,4} \tag{13}$$

This completes our list of input parameters required for the kinetic Monte Carlo simulation to study the Ni-Re alloy in the non-dilute regime.

3.4. Kinetic Monte Carlo results

The vacancy diffusion coefficients in non-dilute Ni-Re alloys was calculated using our kMC code. The Ni as well as the Re diffusion coefficients were also calculated. The code is capable of handling an *fcc* simulation cell of size $\geq 4\times4\times4$ with one vacancy for any desired composition, temperature and duration of kMC simulation. It is noteworthy that instead of tracking the atomic coordinates throughout the simulation, only the displacements are calculated for every individual atom and the vacancy from their initial and final position within a kMC segment. The actual vacancy concentration, x_{v} in pure Ni, corresponding to a $\Delta E_{\mathrm{f},Ni}$ value of 1.44 eV [11] has been used in Equation 4 for simplicity. The results presented in this chapter have been calculated for $15 \times 15 \times 15$ supercells for five different temperatures (1173 K - 1573 K).

Table 4: The calculated total energies and vacancy formation energies in pure Ni, $\Delta E_{\mathrm{f},Ni}$ for different simulation cell sizes

Simulation cell size	Energy (eV) (w/o vacancy)	Energy/ atom (eV)	Energy (eV) (with vacancy)	$\Delta E_{\mathrm{f},Ni}$ (eV)
$4 \times 4 \times 4$	-1402.31	-5.48	-1395.56	1.28
$10 \times 10 \times 10$	-21911.16	-5.48	-21904.40	1.28
$15 \times 15 \times 15$	-73950.15	-5.48	-73943.40	1.27
$20 \times 20 \times 20$	-175289.25	-5.48	-175282.49	1.28

3.4.1. Results in pure Ni

The pure Ni energy was calculated as -5.48 eV per atom (pure Re energy was calculated as -13.39 eV per atom) from the implementation of the cluster expansion in the kMC code. This value was constant and did not vary with the simulation cell size. However, this is 0.03 eV lower than that calculated by the CASM code (see Table 2). We believe that this difference was due to the difference in the levels of accuracy used in the two calculations. We used double precision numbers in our kMC code and used the ECIs (see Table 1) without rounding off any digits. The vacancy formation energy of 1.28 eV was predicted from a combination of the binary Ni-Re cluster expansion and EVFE. These numbers have been tabulated for 4 different simulation cell sizes (see Table 4). Also $\Delta E_{\mathrm{m},i}$ value for Ni was 1.08 eV from Equation 12 on KRAs, same as the results from the first principles calculations.

Given that all these numbers were fairly accurate, we calculated D_{v} in pure Ni by running kMC simulations for a total of 10^9 (1 billion) vacancy jumps. A kMC segment length of 10000 jumps matched best with the results of the analytical formulations. Hence, a segment length of 10000 was used in all the following calculations. It was concluded that the kMC code works correctly as it was successful in replicating a vacancy correlation factor ≈ 1 in the case of pure Ni. It means the vacancy did indeed undergo a 'random walk' in our kMC simulation.

The Ni self-diffusion coefficient was also calculated and this has been plotted in Figure 3 as a function of temperature. The results completely overlap with our previous results from analytical formulations [11] as well as with the kMC simulations of Schuwalow et al [13]. Also, a correlation factor of 0.781 [47] was reproduced in pure Ni reaffirming the validity of the code. The results were within an order of magnitude when compared to the experimental values obtained by Bakker [48]. Similarly, the solute diffusion coefficient of Re in Ni was also calculated for the dilute case using a single Re atom in a $15 \times 15 \times 15$ supercell or an equivalent Re concentration of 0.0074 at.%. This has been shown in Figure 4 and on comparison with Figure 3 it can be seen that Re diffusion coefficient values are approximately two orders of magnitude lower than Ni self-diffusion coefficient values. The results match very well with the results from analytical formulations [11, 49] as well as to the kMC results for dilute alloys [13]. The results were an order of magnitude lower when compared to the experimental interdiffusion coefficients $\tilde{D}$ obtained by Karunaratne et al [50] in dilute alloys of Re in Ni. To a first approximation, $\tilde{D}$ values converge to the solute diffusion coefficient values for the case of dilute alloys, however the underlying assumption is that the thermodynamic factor in Darken's second equation [51] is equal to unity. Thus differences of an order of magnitude are expected when comparing the values.

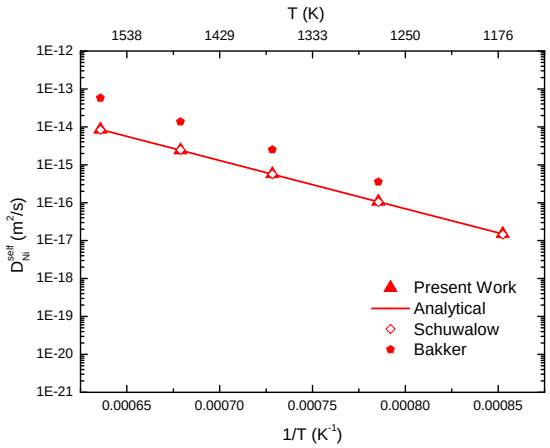

Figure 3: The Ni self-diffusion coefficient calculated as a function of temperature from the kMC simulations in the present work compared to the results calculated from analytical formulations by the authors previously [11], the kMC simulations of Schuwalow et al [13] for dilute alloys and the experimental results of Bakker [48]

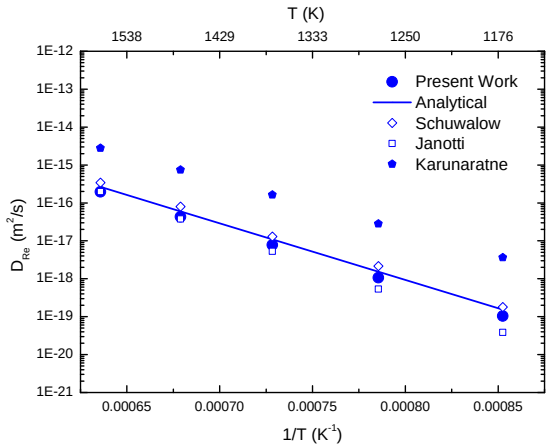

Figure 4: The Re diffusion coefficient in Ni calculated as a function of temperature from the kMC simulations in the present work compared to the results calculated from analytical formulations by the authors previously [11] and Janotti et al [49], the kMC simulations of Schuwalow et al [13] for dilute alloys and the experimental results of Karunaratne et al [50]

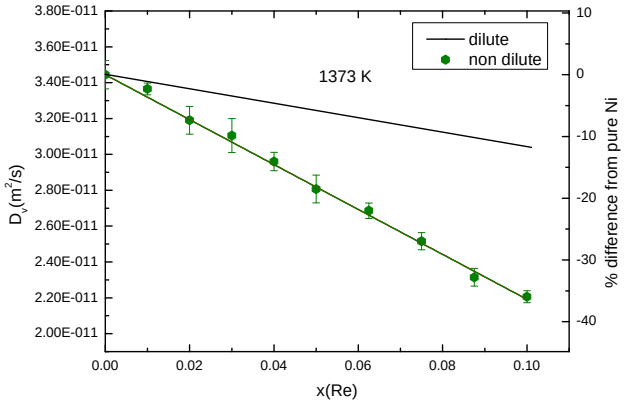

Figure 5: Calculated D_{v} in the non-dilute regime in Ni-Re at 1373 K compared to that obtained using analytical formulations in dilute range[11]

3.4.2. Results in non-dilute Ni-Re alloys

It must be pointed out that the kMC simulations performed in pure Ni only took a few minutes to complete 1 billion vacancy jumps. This was because the energy of the simulation cell and the $\Delta E_{\mathrm{m},Ni}$ both remain fixed. However in the case of non-dilute alloys of Ni-Re, the energy and the $\Delta E_{\mathrm{m},i}$ have to be calculated at each step.

kMC simulations were run for the non-dilute Ni-Re alloys for 15 million vacancy jumps. These simulations running on single processors took 36 hours on an average to complete. The compositions probed were 1 at.%, 2 at.%, 3 at.%, 4 at.%, 5 at.%, 6.25 at. %, 7.5 at.%, 8.75 at. % and 10 at.% Re in binary alloys with Ni. This was because the concentration of Re in the γ phase even in the third generation of most Ni-based superalloys does not exceed 10 at.% [45]. Multiple trials were run for each of these compositions for better statistics.

Figure 5 shows the calculated vacancy diffusion coefficients in the non-dilute regime at 1373 K. Several kMC simulations were run for each composition and the mean D_{v} was calculated. The variation in the results was small, as can be seen from the error bars in Figure 5, where the error bars represent the standard deviation from the mean D_{v}. A linear trend was observed for the entire composition range. An addition of 10 at.% Re is expected to reduce the D_{v} in Ni by 36 %. This is clearly much larger than that predicted by extrapolating the data from our previous work [11] using Manning's random alloy model where 10 at.% Re is expected to reduce the D_{v} in Ni by only 12 % (see Figure 5).

The same trend was observed at other temperatures albeit the reduction in D_{v} becomes smaller with increasing temperature. From the obtained results, D_{v} can be described using the following equation:

$$D_{\mathrm{v}} = D_{\mathrm{v}}^{\mathrm{Ni}}(1 + m x_{\mathrm{Re}}) \tag{14}$$

where D_{v} is the vacancy diffusion coefficient as a function of Re composition x_{Re}, $D_{\mathrm{v}}^{\mathrm{Ni}}$ is the vacancy diffusion coefficient in pure Ni and m is the calculated slope. The values for $D_{\mathrm{v}}^{\mathrm{Ni}}$ and m have been tabulated in Table 5 for

Table 5: The vacancy diffusion coefficient in pure Ni and the calculated slope for D_v as a function of temperature

Temperature (K)	D_v^{Ni} (m^2/s)	m
1173	7.3E-12	-4.14
1273	1.7E-11	-3.84
1373	3.4E-11	-3.60
1473	6.4E-11	-3.47
1573	1.1E-10	-3.14

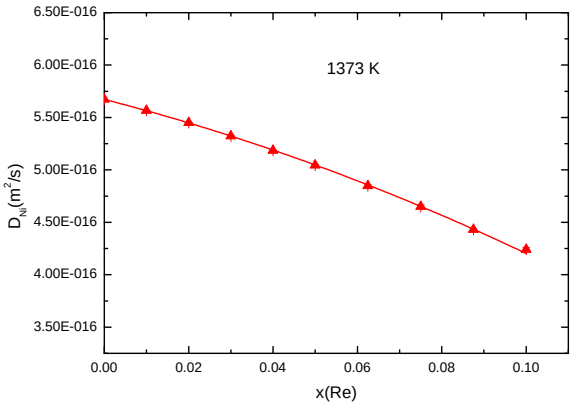

Figure 6: Calculated D_{Ni} in the non-dilute regime in Ni-Re at 1373 K

various temperatures.

The diffusion coefficients of Ni and Re were also calculated in the non-dilute regime, besides the vacancy diffusion coefficients. The results at 1373 K have been shown in Figure 6 and Figure 7 for Ni and Re respectively. The error bars representing the standard deviation of D_{Ni} for the various trials were negligible, while the error bars for D_{Re} were comparatively larger. This was expected as the number of Ni atoms present in the simulation cells were much larger as compared to the number of Re atoms, and hence better statistical averages were obtained for the case of D_{Ni}. A deviation from linearity was seen in both D_{Ni} as well as D_{Re} as a function of Re composition, however the effect was more pronounced for D_{Re}. While the D_{Ni} values decreased with Re concentration monotonically, the D_{Re} values stayed almost constant up to about 3 - 4 at.% before decreasing in magnitude. This meant that up to this concentration, the Re diffusion is not affected by the presence of other Re atoms and that the Re-Re interactions become sizeable only beyond this concentration.

Empirically, the effect of solute concentration on the self-diffusion coefficient of the solvent and the solute diffusion coefficient in the non-dilute alloys have been described using formulations similar to Equations 15 and 16 respectively [15, 16]. For the case of D_{Ni}, we have

$$D_{Ni} = D_{Ni}^{self}(1 + b_1 x_{Re} + b_2 x_{Re}^2 + \dots) \tag{15}$$

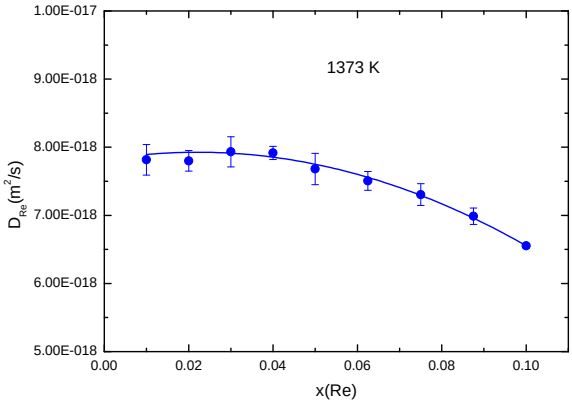

Figure 7: Calculated D_{Re} in the non-dilute regime in Ni-Re at 1373 K

Table 6: The self-diffusion coefficient in pure Ni and the calculated solvent enhancement factors for D_{Ni} as a function of temperature

Temperature (K)	$D_{\mathrm{Ni}}^{\mathrm{self}}$ m^2/s	b_1	b_2
1173	1.50E-17	-2.22	-9.81
1273	1.06E-16	-2.02	-8.06
1373	5.67E-16	-1.82	-7.67
1473	2.41E-15	-1.68	-6.34
1573	8.51E-15	-1.53	-6.38

where D_{Ni} is the Ni diffusion coefficient as a function of Re composition x_{Re}, while $D_{\mathrm{Ni}}^{\mathrm{self}}$ is the self-diffusion coefficient of Ni, and b_1, b_2 , ... are solvent enhancement factors. It has been argued that b_1 represents the effect of isolated solute atoms on $D_{\mathrm{Ni}}^{\mathrm{self}}$, while b_2 represents the effect of paired solute atoms on $D_{\mathrm{Ni}}^{\mathrm{self}}$ and so on [16]. The term b_1 can be described using analytical formulations [15], however no formulation is available for b_2 and higher order terms. Given a deviation from linearity was clearly observed, we have done a parabolic fit of the D_{Ni} data and considered two terms in the Equation 15. These fitting parameters have been tabulated in Table 6.

Similarly for the case of D_{Re}, we have

$$D_{\mathrm{Re}} = D_{\mathrm{Re}}^{\mathrm{dilute}}(1 + B_1 x_{\mathrm{Re}} + B_2 x_{\mathrm{Re}}^2 + \dots) \tag{16}$$

where D_{Re} is the Re diffusion coefficient as a function of Re composition x_{Re}, while $D_{\mathrm{Re}}^{\mathrm{dilute}}$ represents the Re diffusion coefficient in Ni for the dilute case, and B_1, B_2, ... are solute enhancement factors. The D_{Re} data was also fit to a parabola and these values have been tabulated in Table 7. The values for D_{Re} at the Re concentration of 1 at.% were taken as $D_{\mathrm{Re}}^{\mathrm{dilute}}$ in the present case.

3.4.3. Correlation factors

Calculated f_{v}, f_{Ni} and f_{Re} values for various Ni-Re compositions at 1373 K have been plotted in Figure 8. The trend in f_{v} looks similar to that of D_{v} at 1373 K (see Figure 5). This is expected as D_{v} is directly proportional to f_{v}

Table 7: The Re diffusion coefficient in the dilute case and the calculated solute enhancement factors for D_{Re} as a function of temperature

Temperature (K)	$D_{\mathrm{Re}}^{\mathrm{dilute}}$ m^2/s	B_1	B_2
1173	1.03E-19	0.44	-20.87
1273	1.07E-18	0.73	-23.99
1373	7.82E-18	1.28	-28.95
1473	4.29E-17	1.39	-27.92
1573	1.95E-16	1.40	-27.23

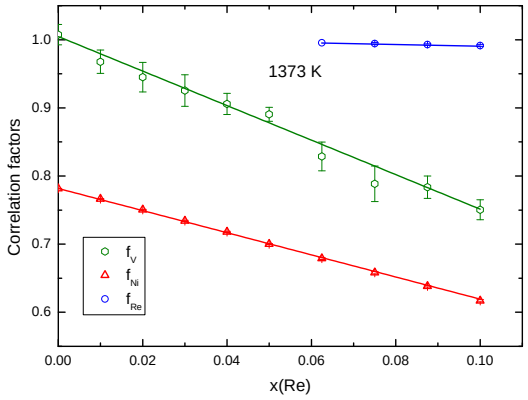

Figure 8: Calculated correlation factors in the non-dilute regime in Ni-Re at 1373 K

[11]. f_{v} is close to unity for pure Ni, and the value gradually drops with increasing Re concentration. However, the decrease in f_{v} is more pronounced than that predicted by the Manning's model [11] which predicted a negligible effect of Re concentration on f_{v}. An addition of 10 at.% Re brings down the f_{v} to approximately 0.75, implying moderate correlation effects.

An f_{Ni} value of 0.781 was calculated for pure Ni, which matches the value in the literature accurately [47]. The f_{Ni} value decreased linearly with the Re concentration to about 0.62 for 10 at.% Re. This is expected as a reverse jump after a Ni-vacancy exchange becomes more likely if the Ni atom is surrounded by more Re atoms, given the low value for the Re-vacancy exchange frequency. As a result, the efficiency of the Ni diffusion is reduced.

In the case of Re, the f_{Re} values could not be calculated up to 5 at.% Re. This is because given the low frequency for a Re-vacancy exchange owing to the high migration barrier [11], if the Re atoms do not perform a single jump in an entire kMC segment, the f_{Re} value for that segment becomes undefined, thus giving an error in the overall f_{Re} value. This becomes less likely with increasing Re concentration, as is seen to be the case beyond 5 at.% Re. This is in contrast to the calculation of D_{Re}, where the mean of the squared displacement is taken over all the Re atoms in the system, thus giving a well-defined value even for the case of dilute alloys. The calculated f_{Re} value was 0.995 for 6.25 at.% Re and dropped only to 0.991 for 10 at.% Re. Thus, effectively the Re diffusive jumps were uncorrelated throughout the investigated composition range, which matches the results from analytical formulations [11].

3.5. Discussion

Having calculated the vacancy diffusion coefficients in the non-dilute regime for Ni-Re alloys, its application to a creep model needs to be verified. It must be reiterated that Ni-based superalloys are used in high temperature applications where creep is the main deformation mechanism. It has been found that the creep strain rate $\dot{\epsilon}$ is inversely proportional to the time to rupture t_r of the superalloy component. Thus, we have

$$\dot{\epsilon} \times t_r = B \tag{17}$$

where B is a constant. This is called the Monkman-Grant relationship [1]. Also, from our hypothesis, the vacancy diffusion coefficient D_v is proportional to the effective diffusion coefficient D_{eff}. Thus using Equation 1, we have

$$D_v \propto D_{eff} \propto \frac{1}{t_r} \tag{18}$$

We use this relationship to validate the creep results of Blavette et al[52] conducted on two different Ni-based superalloys, CMSX-2 and PWA 1480 at a temperature of 1123 K and an applied stress of 500 MPa. Re additions were made to these first generation superalloys at the expense of W partially or completely. The corresponding Re composition in the γ phase, x_{Re} and time to rupture, t_r for these superalloys before and after Re addition have been tabulated in Table 8. The superalloy samples were heat treated at the same temperature as the creep tests, and hence the x_{Re} values represent the actual Re composition of the alloy at the creep temperature. Given that all other factors remain unchanged, the increase in creep lives should be attributed to the change in D_v by the Re addition. Table 9 shows the D_v values calculated in the binary Ni-Re alloys for pure Ni, 3 at.% Re and 4 at.% Re at 1173 K, which closely resemble the investigated superalloys. The calculated decrease in D_v accounts for about three-fifth of the decrease in ${t_r}^{-1}$ in both the cases. This largely explains the origin of the Re-effect in these alloys.

Again, from the calculation of D_v in dilute alloys [11], it was found that W has the same potency as Re as far as reduction in D_v is concerned. Thus, given that Re additions were made to these alloys at the expense of W, one can justify the improvement in creep lives to the fact that Re partitioning to the γ phase is stronger than W. Indeed, while the W concentration in the γ phase of PWA 1480 alloy was 2.15 at.%, on being replaced by Re completely in the PWA 1480+Re alloy, the Re concentration in the γ phase was 3.71 at.%. Thus, the Re-effect should be explained in totality by its slowing down of the vacancy diffusion together with strong partitioning to the γ phase. It must be pointed out that validation of our results would require agreement with more creep data on superalloys from a number of sources. However, it is important to understand that the number of variables in superalloys metallurgy is very large, and hence availability of creep data where most variables have been kept fixed is limited.

The present study in the non-dilute regime helps to improve our understanding of how Re may affect the creep properties in these materials. In terms of future work, there are several areas where the present research can be improved upon. The calculation of non-dilute diffusivities should be extended to treat ternary systems, which would require effective cluster interaction coefficients and kinetically resolved activation barriers fit against a larger dataset.

Table 8: Re composition in γ phase (x_{Re}) and time to rupture (t_{r}) for some superalloys studied by Blavette et al [52] at 1123 K and 500 MPa

Superalloy	x_{Re}	t_{r} (hours)	% decrease in $\left(\frac{1}{t_{\mathrm{r}}}\right)$
CMSX-2	0	382	-
CMSX-2 + Re	0.0287	498	23.3
PWA 1480	0	356	-
PWA 1480 + Re	0.0371	497	28.3

Table 9: D_{v} corresponding to Re composition in binary Ni-Re alloys at 1173 K calculated in the present work

Alloy	x_{Re}	D_{v} (m^2/s)	% decrease in D_{v}
Pure Ni	0	7.30E-12	-
Ni-3 at.% Re	0.03	6.32E-12	13.5
Pure Ni	0	7.30E-12	-
Ni-4 at.% Re	0.04	6.11E-12	16.3

Diffusion calculations, especially in the non-dilute regime must also be performed on other alloying elements commonly added to Ni-based superalloys. This is desirable in order to get a complete picture of the effect of chemistry on creep in superalloys.

4. Conclusion

1. The effect of Re additions on diffusional processes in Ni was investigated to explain how Re composition in γ may affect the climb of dislocations at the γ/γ' interfaces, with ramifications on creep properties.
2. The results were obtained by performing kinetic Monte Carlo simulations based on data obtained from density functional theory.
3. Cluster expansion was employed to calculate the total energy of a configuration of atoms while the values of migration energy barriers were also cluster expanded considering first neighbours only.
4. Results from the non-dilute alloys of Re in Ni suggest that solute-solute interactions have sizeable effects on vacancy diffusivity.
5. Applying the data from a previous experimental work to a simple creep model, the Re-effect was explained in terms of its role on diffusional processes in Ni. However, validation with more experimental data is desirable.

Acknowledgements

The authors would like to acknowledge the use of the *BlueBEAR* high performance computing facility at the University of Birmingham as well as the *MidPlus* regional high performance computing facility for the calculations presented in this manuscript.

References

[1] R. C. Reed. *The superalloys: fundamentals and applications*. Cambridge University Press, 2006.

[2] A. Mottura and R. C. Reed. What is the role of rhenium in single crystal superalloys? *MATEC Web of Conferences*, 14:01001, 2014.

[3] A. Mottura, M. W. Finnis, and R. C. Reed. On the possibility of rhenium clustering in nickel-based superalloys. *Acta Materialia*, 60(6-7):2866–2872, 2012.

[4] A. F. Giamei. Deformation and fracture of advanced anisotropic superalloys. AFOSR Annual Report FR-11009, 1978.

[5] Z. Zhu, H. Basoalto, N. Warnken, and R. C. Reed. A model for the creep deformation behaviour of nickel-based single crystal superalloys. *Acta Materialia*, 60(12):4888–4900, 2012.

[6] B. F. Dyson. Microstructure based creep constitutive model for precipitation strengthened alloys: theory and application. *Materials Science and Engineering: A*, 25(2):213–220, 2009.

[7] C. Herring. Diffusional viscosity of a polycrystalline solid. *Journal of Applied Physics*, 21(5):437–445, 1950.

[8] J. Weertman. Creep of indium, lead, and some of their alloys with various metals. *Transactions of the American Institute of Mining and Metallurgical Engineers*, 218(2):207–218, 1960.

[9] A. Heckl, S. Neumeier, M. Göken, and R. F. Singer. The effect of Re and Ru on γ/γ' microstructure, γ-solid solution strengthening and creep strength in nickel-base superalloys. *Materials Science and Engineering: A*, 528(9):3435–3444, 2011.

[10] A. P. Miodownik, X. Li, N. Saunders, and J. Ph. Schille. Modelling of creep in nickel based superalloys. In A. Strang, editor, *Parsons 2003: Engineering Issues in Turbine Machinery, Power Plant and Renewables*, pages 779–787. Institute of Materials, Minerals, and Mining, Maney Publishing, London, 2003.

[11] K. N. Goswami and A. Mottura. Can slow-diffusing solute atoms reduce vacancy diffusion in advanced high-temperature alloys? *Materials Science and Engineering: A*, 617:194–199, 2014.

[12] J. R. Manning. Correlation factors for diffusion in nondilute alloys. *Physical Review B*, 4:1111–1121, 1971.

[13] S. Schuwalow, J. Rogal, and R. Drautz. Vacancy mobility and interaction with transition metal solutes in Ni. *Journal of Physics: Condensed Matter*, 26(48):485014, 2014.

[14] R. E. Howard and J. R. Manning. Kinetics of solute-enhanced diffusion in dilute face-centered-cubic alloys. *Physical Review*, 154(3):561–568, 1967.

[15] C. L. Zacherl. *A computational investigation of the effect of alloying elements on the thermodynamic and diffusion properties of fcc Ni alloys, with application to the creep rate of dilute Ni-X alloys*. PhD thesis, The Pennsylvania State University, 2012.

[16] A. D. Leclaire. Solute diffusion in dilute alloys. *Journal of Nuclear Materials*, 69-70:70–96, 1978.

[17] I. V. Belova and G. E. Murch. Enhancement of solute self-diffusion in *fcc* alloys. *Philosophical Magazine*, 86(12):1615–1629, 2006.

[18] J. Rogal. *Stability, composition and function of palladium surfaces in oxidizing environments: a first-principles statistical mechanics approach*. PhD thesis, Freie Universität Berlin, Berlin, 2006.

[19] G. H. Vineyard. Frequency factors and isotope effects in solid state rate processes. *Journal of Physics and Chemistry of Solids*, 3(1-2):121–127, 1957.

[20] A. F. Voter. Introduction to the kinetic Monte Carlo method. In K. E. Sickafus, E. A. Kotomin, and B. P. Uberuaga, editors, *Radiation Effects in Solids*, pages 1–23, Springer Netherlands, 2007.

[21] J. R. Norris. *Markov Chains*. Cambridge University Press, 1997.

[22] A. B. Bortz, M. H. Kalos, and J. L. Lebowitz. A new algorithm for Monte Carlo simulation of Ising spin systems. *Journal of Computational Physics*, 17(1):10–18, 1975.

[23] Y. A. Du, J. Rogal, and R. Drautz. Diffusion of hydrogen within idealized grains of *bcc* Fe: a kinetic Monte Carlo study. *Physical Review B*, 86(17):174110, 2012.

[24] M. E. Glicksman. *Diffusion in solids: field theory, solid-state principles, and applications*. John Wiley and Sons, 1999.

[25] J. M. Sanchez, F. Ducastelle, and D. Gratias. Generalized cluster description of multicomponent systems. *Physica A: Statistical Mechanics and its Applications*, 128(1-2):334–350, 1984.

[26] A. Van der Ven and G. Ceder. First principles calculation of the interdiffusion coefficient in binary alloys. *Physical Review Letters*, 94(4):045901, 2005.

[27] A. Van der Ven, J. C. Thomas, Q. Xu, B. Swoboda, and D. Morgan. Nondilute diffusion from first principles: Li diffusion in Li_xTiS_2. *Physical Review B*, 78(10):104306, 2008.

[28] A. Van der Ven, J. C. Thomas, Q. Xu, and J. Bhattacharya. Linking the electronic structure of solids to their thermodynamic and kinetic properties. *Mathematics and Computers in Simulation*, 80(7):1393–1410, 2010.

[29] A. Walle and G. Ceder. Automating first-principles phase diagram calculations. *Journal of Phase Equilibria*, 23(4):348–359, 2002.

[30] A. Van der Ven and G. Ceder. Vacancies in ordered and disordered binary alloys treated with the cluster expansion. *Physical Review B*, 71(5):054102, 2005.

[31] A. Van der Ven, G. Ceder, M. Asta, and P. D. Tepesch. First-principles theory of ionic diffusion with nondilute carriers. *Physical Review B*, 64(18):184307, 2001.

[32] P. Hohenberg and W. Kohn. Inhomogeneous electron gas. *Physical Review*, 136:B864–B871, 1964.

[33] W. Kohn and L. J. Sham. Self-consistent equations including exchange and correlation effects. *Physical Review*, 140:A1133–A1138, 1965.

[34] G. Kresse and J. Furthmüller. Efficient iterative schemes for *ab initio* total-energy calculations using a plane-wave basis set. *Physical Review B*, 54:11169–11186, 1996.

[35] P. E. Blöchl. Projector augmented-wave method. *Physical Review B*, 50:17953–17979, 1994.

[36] G. Kresse and D. Joubert. From ultrasoft pseudopotentials to the projector augmented-wave method. *Physical Review B*, 59:1758–1775, 1999.

[37] J. P. Perdew, K. Burke, and M. Ernzerhof. Generalized gradient approximation made simple. *Physical Review Letters*, 77:3865–3868, 1996.

[38] M. Methfessel and A. T. Paxton. High-precision sampling for Brillouin-zone integration in metals. *Physical Review B*, 40:3616–3621, 1989.

[39] H. J. Monkhorst and J. D. Pack. Special points for Brillouin-zone integrations. *Physical Review B*, 13:5188–5192, 1976.

[40] G. Henkelman and H. Jónsson. Improved tangent estimate in the nudged elastic band method for finding minimum energy paths and saddle points. *The Journal of Chemical Physics*, 113(22):9978–9985, 2000.
[41] G. Henkelman, B. P. Uberuaga, and H. Jónsson. A climbing image nudged elastic band method for finding saddle points and minimum energy paths. *The Journal of Chemical Physics*, 113(22):9901–9904, 2000.
[42] C. Kittel. *Introduction to solid state physics*. John Wiley & Sons, 2005.
[43] S. B. Maisel, N. Schindzielorz, A. Mottura, R. C. Reed, and S. Müller. Nickel-rhenium compound sheds light on the potency of rhenium as a strengthener in high-temperature nickel alloys. *Physical Review B*, 90(9):094110, 2014.
[44] O. Levy, M. Jahnátek, R. V. Chepulskii, G. L. W. Hart, and S. Curtarolo. Ordered structures in rhenium binary alloys from first-principles calculations. *Journal of the American Chemical Society*, 133(1):158–163, 2010.
[45] C. Schulze and M. Feller-Kniepmeier. Transmisson electron microscopy of phase composition and lattice misfit in the Re-containing nickel-base superalloy CMSX-10. *Materials Science and Engineering: A*, 281(1-2):204–212, 2000.
[46] G. L. W. Hart, V. Blum, M. J. Walorski, and A. Zunger. Evolutionary approach for determining first-principles hamiltonians. *Nature Materials*, 4(5):391–394, 2005.
[47] K. Compaan and Y. Haven. Correlation factors for diffusion in solids. *Transactions of the Faraday Society*, 52:786–801, 1956.
[48] H. Bakker. A curvature in the In D versus 1/T plot for self-diffusion in nickel at temperatures from 980 to 1400 °C. *Physica Status Solidi B*, 28(2):569–576, 1968.
[49] A. Janotti, M. Krčmar, C. L. Fu, and R. C. Reed. Solute diffusion in metals: larger atoms can move faster. *Physical Review Letters*, 92(8):085901, 2004.
[50] M. S. A. Karunaratne, P. Carter, and R. C. Reed. Interdiffusion in the face-centred cubic phase of the Ni-Re, Ni-Ta and Ni-W systems between 900 and 1300 °C. *Materials Science and Engineering: A*, 281(1-2):229–233, 2000.
[51] D. A. Porter and K. E. Easterling. *Phase transformations in metals and alloys, third edition (revised reprint)*. Taylor & Francis, 1992.
[52] D. Blavette, P. Caron, and T. Khan. An atom probe investigation of the role of rhenium additions in improving creep resistance of Ni-base superalloys. *Scripta Metallurgica*, 20(10):1395 – 1400, 1986.